

# Simulation of Water Loading On Deformable Structures Using SPH

J.C. Campbell<sup>1</sup>, R. Vignjevic<sup>1</sup>, M. Patel<sup>1</sup> and S. Milisavljevic<sup>1</sup>

**Abstract:** This paper presents research towards the development of an analysis technique for predicting the interaction of large ocean waves with ships and offshore structures specifically with respect to the extent of deck submersion, impact loads and the level of structural damage caused. The coupled SPH – Finite Element approach is used, where the water is modeled with SPH and the structure with shell or continuum finite elements. Details of the approach are presented, including the SPH-FE contact and the fluid boundary conditions. Simulation results show that the method can correctly represent the behavior of a floating structure and the structural response to water impact.

**Keywords:** SPH, finite element, green water, wave impact.

## 1 Introduction

Green water loading, meaning deck submergence on ships and offshore structures, and wave impact are major sources of damage in the marine industry. Design for such eventualities is based on empirical considerations and on model test data in the absence of reliable theoretical models for predicting the relevant loads.

Smooth Particle Hydrodynamics (SPH) is a numerical technique for the approximate integration of partial differential equations. It is a meshless Lagrangian method that uses a pseudo-particle interpolation method to compute smooth field variables. Each pseudo-particle has a mass, Lagrangian position, Lagrangian velocity, and internal energy; other quantities are derived by interpolation or from constitutive relations. Gingold and Monaghan (1977) and Lucy (1977) initially developed the SPH approach for the simulation of astrophysics problems. Their breakthrough was a method for the calculation of derivatives that did not require a structured computational mesh. Review papers by Benz (1990) and Monaghan (1992) cover the early development of SPH. Libersky and Petchek (1990) extended SPH to work with the full stress tensor, developing a 2D formulation. This addition

---

<sup>1</sup> School of Engineering, Cranfield University, UK.

allowed SPH to be used in problems where material strength is important and lead to further developments of the method, including the linking of SPH with existing finite element codes [Johnson (1994)] [Attaway, Heinstein and Swegle (1994)] [Vignjevic, Reveles and Campbell (2006)].

The application of SPH to water waves and related free-surface hydrodynamics problems was begun by Monaghan (1994), who presented two-dimensional results for a dam break problem and wave propagation onto a shallow beach. In more recent work, Monaghan has compared SPH simulations with published experimental results for Scott Russell's wave generator, gravity currents traveling down a ramp in a tank stratified in two layers and wave run-up and return on a beach. In all three cases he shows that the SPH method is in agreement with the experimental results. All these simulations use an artificial equation of state to produce a quasi-incompressible fluid. SPH has also been used for wave mechanics with exact enforcement of incompressibility [Lo and Shao (2002)]. This uses an implicit pressure update that allows a larger time step but requires more computational work per time step. Recently SPH methods have been successfully applied to 2D simulations of water behavior, including wave overtopping, using rigid representations of the impacted structure [Gómez-Gesteira, Cerqueiro, Crespo, and Dalrymple (2005)] [Shao, Ji, Graham, Reeve, James and Chadwick (2006)] [Crespo, Gomez-Gesteira and Dalrymple (2007)], and 3D simulations, including a dam break problem [Moulinec, Issa, Marongiu and Violeau (2008)].

Other meshless methods have been used for incompressible flows, including the Moving Particle Semi-implicit (MPS) method [Koshizuka, Nobe and Oka (1998)] [Xie, Koshizuka and Oka (2007)], which is related to the SPH method. The pressure is implicitly calculated from Poisson's equation in order to deal with incompressibility. The MPS method has been extended to model the interaction of fluids with elastic and visco-plastic structures [Chikazawa, Koshizuka and Oka (2001)]. However the structures that it is applied to are simple, solid models, no structural elements are used and overall deformations are small.

Other approaches for wave impact simulations typically use Eulerian or ALE methods to solve the Navier-Stokes equations. Aliabadi, Abedi, Zellars, Bota and Johnson (2003) have used an unstructured mesh finite element method to simulate wave breaking and wave impact on rigid circular columns. Buchner, Kleefsman and co-workers [Buchner, Bunnik, Fekken and Veldman (2001)] [Kleefsman, Fekken, Veldman, Bunnik, Buchner and Iwanowski (2002)] have developed an Eulerian code and applied it to wave run-up and green water loading on Floating Production Storage and Offloading (FPSO) systems. They show good agreement with experiment for structural loads, but again the structures are represented by rigid shapes.

For ships and offshore structures the goal is a reliable technique for predicting

the structural response to extreme wave loads. This is a complex problem involving the interaction of non-linear fluid behavior (breaking waves, fluid impact) with non-linear structural behavior (large deformations, contact, material plasticity and damage). The explicit finite element method is the established method for simulating the crash and impact response of structures and is implemented in numerous commercial and development codes, see for example DYNA3D [Lin (1999)]. Due to the well known problems with mesh-tangling this method is not appropriate for modeling the fluid and the method must be coupled with another method, such as SPH, appropriate for modeling the fluid behavior.

Previous work by De Vuyst, Vignjevic and Campbell (2005) has developed and demonstrated a contact algorithm for coupling meshless and finite element discretisations, allowing complex interaction in three dimensional simulations. A primary application of this method was the simulation of helicopter crash on water and it has been demonstrated for the impact of rigid and deformable structures on water [De Vuyst (2003)]. Extend this approach to wave loading of offshore structures required development of appropriate initial and boundary conditions for the fluid component. All developments were implemented within the existing tool which consists of the LLNL-DYNA3D code [Lin (1999)] coupled to a 3D SPH solver developed at Cranfield University. The SPH solver uses the same explicit central-difference time integration algorithm as LLNL-DYNA3D.

This paper describes research towards a modeling approach allowing the modeling of wave interaction with a deformable structure using an explicit coupled SPH-finite element approach. The specific developments required to allow the coupled approach to model the interaction of a floating structure with waves are discussed. Then specific simulation results are shown that test the ability of the method to correctly represent two key aspects of this problem: correct behavior of a floating body and large structural deformation due to water impact. The specific test problems were selected based on the availability of published results for comparison. The behavior of a floating body is tested through comparison with published numerical results obtained using an Eulerian solver. The results of a water impact simulation are then presented to show that the coupled FE-SPH method allows large structural deformation.

## **2 Coupling between the SPH and FE solvers**

This section gives an overview of the SPH method for modeling water behavior and the contact algorithm between the SPH and FE solvers. This will be brief as the method detailed descriptions are available, see for example Monaghan (1994) and De Vuyst, Vignjevic and Campbell (2005).

The SPH method uses a set of nodes, or particles, to represent a material, no mesh or structure is required to calculate the derivatives of a field. A kernel function,  $W$ , centered at each particle provides the weighting function used for interpolation. The kernel function has compact support and is non-zero within a radius of  $2h$  from the particle location. The length  $h$  is known as the smoothing length and controls the support of each particle.

A consequence of the SPH method is that the location of the boundary of a solid or liquid is not well defined. Each particle is the centre of a sub-domain with radius  $2h$  and consequently the boundary is diffused over this length. To avoid the requirement to construct a surface geometry from the SPH nodes a contact potential based on the kernel function is used [De Vuyst, Vignjevic and Campbell (2005)][Vignjevic, De Vuyst and Campbell (2006)]. This potential is defined as

$$\phi_x(x_A) = \int_{\Omega_c} K \left( \frac{W(x_A - x_B)}{W(\Delta p_{avg})} \right)^n dV, \quad (1)$$

then a discrete form of the contact potential is used to define the contact force:

$$f_c(x_A) = \frac{m_A}{\rho_A} \sum_B^{NCONT} \frac{m_B}{\rho_B} K n \frac{W(x_A - x_B)^{n-1}}{W(\Delta p_{avg})^n} \nabla W(x_A - x_B). \quad (2)$$

Here  $x_A$  and  $x_B$  are the coordinates of two particles in different bodies,  $\Delta p_{avg}$  denotes the average node spacing in the neighborhood of particle  $A$ . The user defined parameters are  $K$  and  $n$ . These parameters provide control over the contact force and hence the distance between particles in the two bodies at which contact equilibrium is established. In all simulations a value of 4 for the non-dimensional parameter  $n$  has been used. The parameter  $K$  has the dimension of stress and is problem dependent, a value in the range of 10-50Pa has been found to be effective in typical water impact problems.

In applying this contact potential to contact between FE and SPH, the contact force is applied between an SPH particle and FE node that lies within  $2h$  of that particle, see Fig. 1.

Under the conditions of wave loading the water can be considered incompressible. The SPH solver used assumes that all materials are compressible and therefore a bulk stiffness, in the form of an equation of state (EOS), must be defined. In this paper, unless stated otherwise, the Murnaghan EOS is used for the water. This has the form

$$P = B \left[ \left( \frac{\rho}{\rho_0} \right)^\gamma - 1 \right], \quad (3)$$

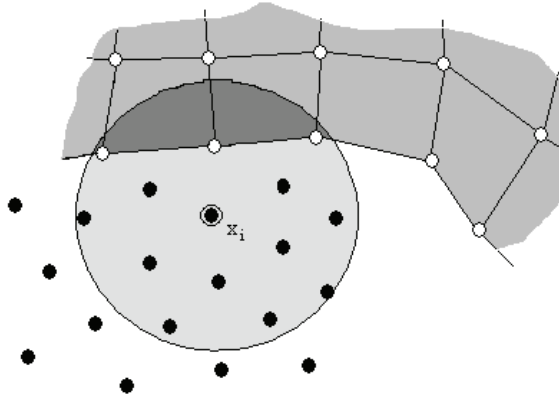


Figure 1: SPH particle at point  $x_i$  interacts with all FE nodes within  $2h$ , denoted by light grey circle.

where  $B$  and  $\gamma$  are user supplied material coefficients. Following Monaghan (1994) a value of  $\gamma=7$  is used and the parameter  $B$  is chosen to give an artificially low speed of sound, while keeping the density changes small. This is valid provided the flow velocities are small compared with the speed of sound [Monaghan (1994)]. The advantage of this is that a lowered speed of sound increases the critical time step size for the explicit time integration algorithm, potentially reducing the CPU cost of a simulation.

### 3 SPH for wave loading

Simulation of wave loading requires significantly more complex initial and boundary conditions for the water component than required for the impact of a structure on water considered previously [DeVuyst (2003)][De Vuyst, Vignjevic and Campbell (2005)].

#### 3.1 Initial conditions

At the start of the simulation the problem must be under static equilibrium. If it is not the initial behavior of the model will be governed by this lack of equilibrium, potentially obscuring the behavior of interest. The initial equilibrium must be determined for

- Pressure vs. depth in the water

- Initial contact forces between structure and water. This is particularly critical for floating bodies.

The pressure-depth relationship can be determined analytically for a given equation of state, therefore it is possible to determine the correct density for each particle. The initial contact forces can not be determined analytically due to its non-linear dependence on the relative positions of the SPH particles and FE nodes. Consequently a numerical technique was required to determine the initial state of a problem.

The dynamic relaxation method was selected to solve the initial static problem. Dynamic relaxation is a commonly used method that allows an explicit transient solver to approximate the solution to a static problem, see for example [Lin (1999)]. It achieves this by introducing an artificial damping term into the dynamic equilibrium equation

$$\mathbf{M}\ddot{\mathbf{x}}^n + \mathbf{C}\dot{\mathbf{x}}^n + \mathbf{K}\mathbf{x}^n = \mathbf{F}^n, \quad (4)$$

where  $\mathbf{C}$  is the damping matrix. For dynamic relaxation  $\mathbf{C}$  has the form [Hallquist (2006)]:

$$\mathbf{C} = c\mathbf{M}. \quad (5)$$

where  $c$  is a scalar multiplier to the mass matrix  $\mathbf{M}$ . This definition of the damping matrix ensures that  $\mathbf{C}$  is diagonal as required by the explicit central difference algorithm. In practice the damping is introduced through a modification of the velocity update step of the time integration algorithm [Hallquist (2006)]. The modified equation is

$$\dot{\mathbf{x}}^{n+1/2} = \eta\dot{\mathbf{x}}^{n-1/2} + \dot{\mathbf{x}}^n\Delta t^n, \quad (6)$$

where  $\eta$  is the damping factor (a value of 0.995 was used) and the superscripts refer to the time level at which the parameter is measured. The simulation continues until the solution converges. Convergence is determined by monitoring the global kinetic energy of the simulation and is assumed to occur once

$$KE < tol \cdot KE_{\max}. \quad (7)$$

The tolerance,  $tol$ , is usually taken as 0.001. This value has been used in this work. The existing dynamic relaxation algorithm in DYNA3D was extended to include the SPH solver. Due to the computational cost of the dynamic relaxation solution on 3D coupled simulations the coupled solver was extended to allow the state at the

end of the dynamic relaxation simulation to be saved to a file and later used as the initial condition of a transient simulation.

Figure 2 shows the initial and final states of a dynamic relaxation simulation of a 2D simulation to determine the floating equilibrium of a rigid square with a density of half the water density. In this simulation, rotation of the square flat was prevented. The final state shows the correct pressure depth profile in the water and contact equilibrium between the water and float.

### 3.2 Boundary conditions

During the simulation an appropriate boundary condition is required to generate the waves in the water. If the simulation is required to progress beyond the interaction of the first wave with the structure a non-reflective boundary condition is necessary. Without such a boundary condition the CPU cost of a 3D simulation quickly becomes prohibitive due to the extent of the water domain required.

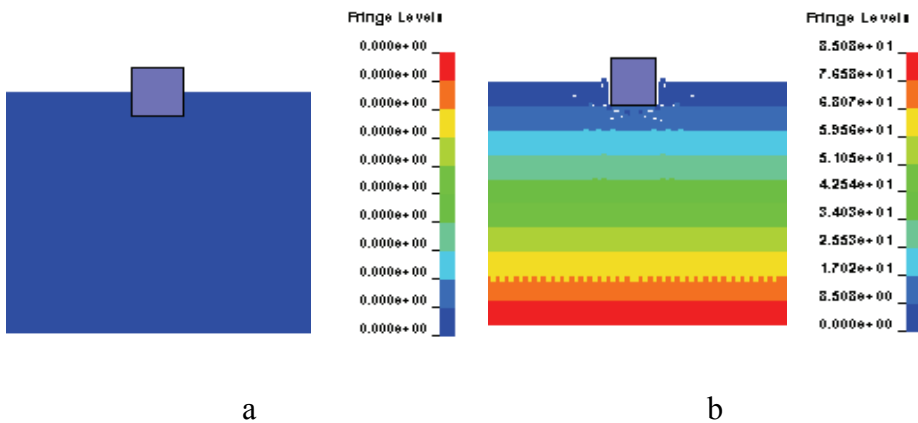


Figure 2: Initial (a) and final (b) state of a dynamic relaxation analysis of a square float. Fringes of pressure (Mbar) are shown.

Where only a single wave is required, and it is not necessary for the structure to be in initial contact equilibrium with the fluid, the initial conditions in the water can be determined from standard wave theory, see for example [Tucker and Pitt (2001)]. Where multiple waves are required or the fluid and structure must be in initial equilibrium the waves have to be generated during the transient analysis. This is achieved through the use of a wave maker that consists of an oscillating plate. This is a copy of wave makers commonly used in experimental wave tanks and is a technique established for numerical wave simulations [Monaghan (1994)]

[Gómez-Gesteira, Cerqueiro, Crespo, and Dalrymple (2005)] [Shao, Ji, Graham, Reeve, James and Chadwick (2006)].

Non-reflecting boundary conditions for pressure waves are well established for Lagrangian hydrocodes, but can not be adapted for water surface waves as the propagation of these waves involves large fluid motion. For deep water a marker particle at the water surface would travel a circular path, with diameter equal to the amplitude of the wave, and any absorbing boundary condition must not prevent this motion. Experimental wave tanks typically use a sloping shore or an active boundary wall to provide a non-reflecting boundary. A sloping shore could be included in the SPH simulation, but would require a significant increase in the size of the water domain and a proportional increase in the computational time. A model of an active boundary wall would be complex to develop and implement numerically.

A non-reflecting boundary condition for water waves has been developed that consist of an additional region of fluid where the motion is damped through the addition of an artificial damping term in to the governing equation. As with dynamic relaxation, in practice the damping is introduced through a modification in the velocity update step, equation (6). Within the damping region the damping factor,  $\eta$  is proportional to the distance from the inlet face of the damping volume,  $x_d$ , as follows:

$$\eta = 1 - \frac{x_d}{l_d}. \quad (8)$$

A value for  $l_d$  of 2.5 to 3 times the wave length of the waves to be absorbed was found to be effective. The rear face of the damping volume can then treated as a rigid wall and placed approximately one-half the wave length from the inlet face as by this point the motion of the water particles is small. SPH particles are free to enter and leave the volume, so it does not prevent the circular motion of the water particles. While this does result in additional computational cost the volume of the damping region should remain small compared with the overall domain.

Comparing the results for a rigid boundary, figure 3a, to the non-reflective boundary, figure 3b, shows a significant difference in behavior. For the non-reflecting boundary the marker particle shows the expected circular motion throughout the simulation, while reflection off the rigid boundary significantly changes the wave behavior later in the simulation.

#### 4 Numerical tests and demonstrations

A set of test cases of varying complexity have been performed to validate the capability of the coupled FE-SPH approach to simulate floating bodies and impact on

water. This section presents some main tests cases from this process. Full demonstration of the method for 3D simulation of extreme wave loading remains to be completed.

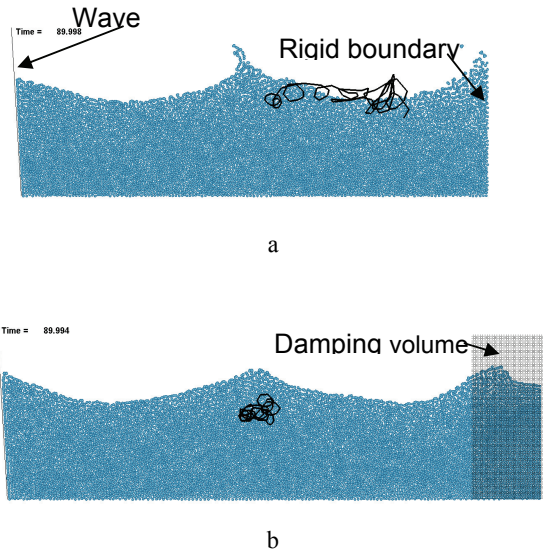


Figure 3: (a) 2D wave tank results with a rigid boundary showing the motion of a marker particle. The initial circular motion of the particle changes as a standing wave system is formed next to the rigid boundary. (b) Results for the same problem using a non-reflective damping layer. The motion of the marker particle remains circular.

#### 4.1 Equilibrium of floating objects

A useful verification of the method's ability to simulate the response of a floating body is to demonstrate that it will reach its correct equilibrium state. Three test cases were selected for which published results [Fekken (2004)], are available. The results were obtained using an Eulerian solver coupled with rigid shapes.

In the first case a 10cm x 10cm square rigid float, with density half the density of the fluid, is in initial unstable equilibrium as shown in figure 4. The fluid domain is 30cm wide by 15 cm deep and contains 6,400 SPH particles with an initial inter-particle spacing of 0.25cm. The element size of the FE mesh used to represent the rigid body is also 0.25cm. While this mesh resolution is far higher than required for a rigid body, it is a requirement of the contact algorithm that the SPH and FE spatial resolutions are similar.

An additional consideration is that this mesh resolution is representative of the mesh resolution required when considering a deformable structure.

Dynamic relaxation is used to determine the static solution to the initial pressure and contact equilibrium using additional constraints to prevent rotation of the float. In the simulation the float rotates through 45 degrees to the stable equilibrium, figure 5, and settles in that state after a period of damped oscillation. A comparison between the current results and the Eulerian results [Fekken (2004)] is shown in Figure 6, showing good agreement. The zero time for the current results has been shifted so that the time of initial rotation agrees as the published results used an initial rotational velocity as a disturbance, while no initial disturbance was used in the current work.

A second test was run using the square float, with the density of the square reduced to one quarter that of the fluid. The initial conditions of the simulation were identical to the half density case, so the float will initially rise before settling down to its stable equilibrium position, figure 7. For this problem the theoretical value for the final angle of rotation is 63.4 degrees. In the simulation the float, after oscillation, settles down to approximately 63 degrees, figure 8.

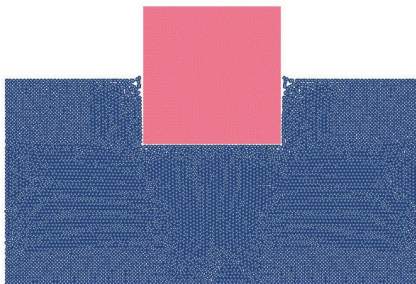


Figure 4: Initial unstable equilibrium position of square float with density half the density of the fluid.

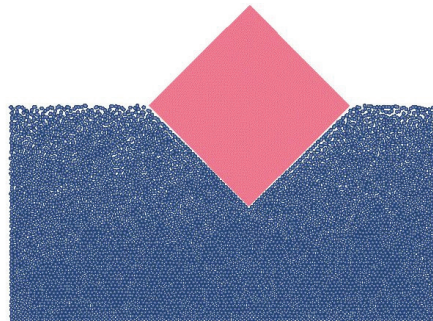


Figure 5: Final equilibrium position of square with density half the density of the fluid.

The third test used a rectangular float, 10 cm x 5 cm, with density half the density of the fluid. The initial position of the float is with the long axis vertical, with the initial unstable equilibrium determined by a dynamic relaxation simulation to determine the pressure and contact equilibrium, figure 9. In this model the size of the fluid domain has been extended to 50cm wide and 25cm deep in order to prevent the boundaries from influencing the float behavior. The spatial resolutions remain constant with 19,600 SPH particles used for the fluid. In the simulation the

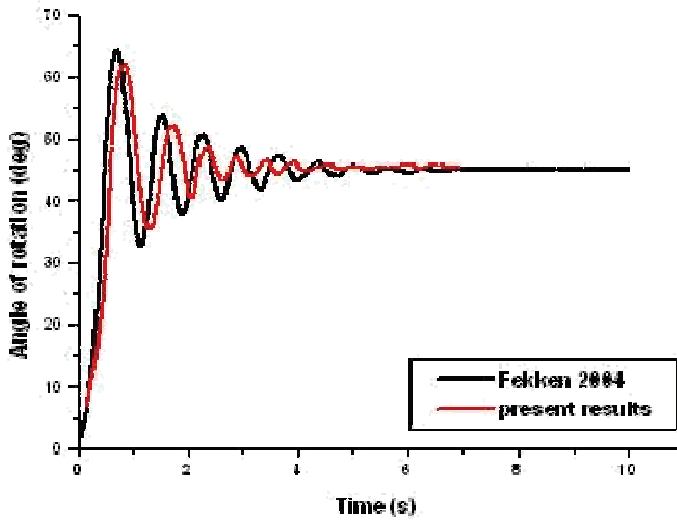


Figure 6: Time history of rotation angle of square float. The present results have been shifted to match the start of rotation due to different initial perturbations in the two simulations.

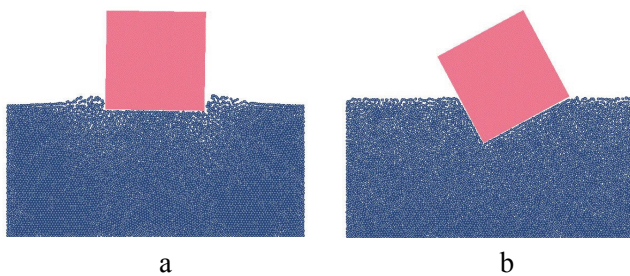


Figure 7: The square float initially rises (a) before settling to the final equilibrium position (b)

float rotates to the stable equilibrium position with the long axis horizontal, figures 10 and 11.

These results from these tests show that the coupled FE-SPH approach will correctly predict the equilibrium floating behavior of a floating body.

## 4.2 Rising cylinder

In the final 2D test presented in this paper, a cylinder of radius 1m is initially submerged and is released to rise to the surface. The cylinder has density 0.6 times the fluid density and the centre of mass is initially at a depth of 5m. Dynamic relaxation is used to determine the static solution to the initial pressure and contact equilibrium. The results show the cylinder rising through the fluid, figure 12a, and then breaking through the fluid surface, figure 12b. This test case is used for Eulerian codes to demonstrate the ability of a shape to break through a free surface. This is not an issue for the SPH method as the location of the free surface is determined naturally by the particle positions and does not require special treatment. The velocity of the cylinder agrees well with the published Eulerian results [Fekken (2004)] showing that the coupled approach can correctly treat the buoyancy of a submerged object.

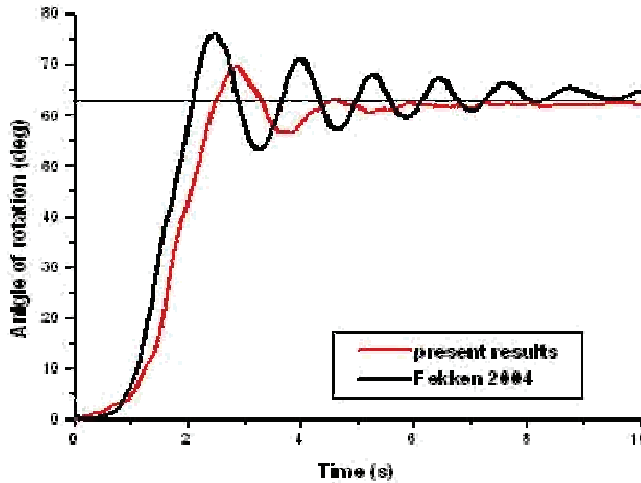


Figure 8: Time history for float with density one quarter the density of the fluid. The horizontal line on the graph marks the theoretical final angle of 63.4 degrees.

## 4.3 Impact of a deformable structure with water

As discussed earlier a specific strength of the coupled FE-SPH approach is that it allows for fluid-structure interaction even when the structure is undergoing large non-linear deformation. The availability of appropriate tests cases for this behavior is limited, so for this work the impact of a metallic helicopter sub-floor structure with water has been selected as experimental data was available.

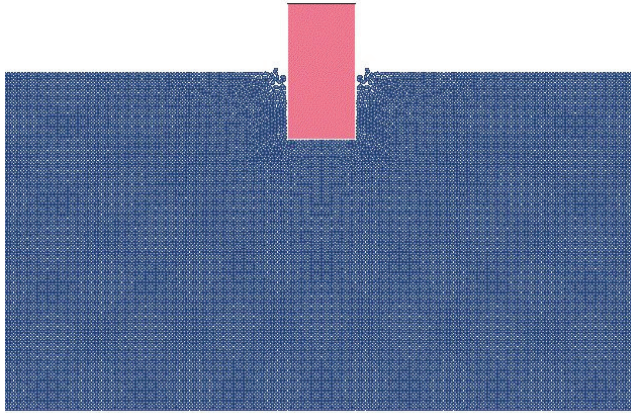


Figure 9: Initial unstable equilibrium position of rectangular float.

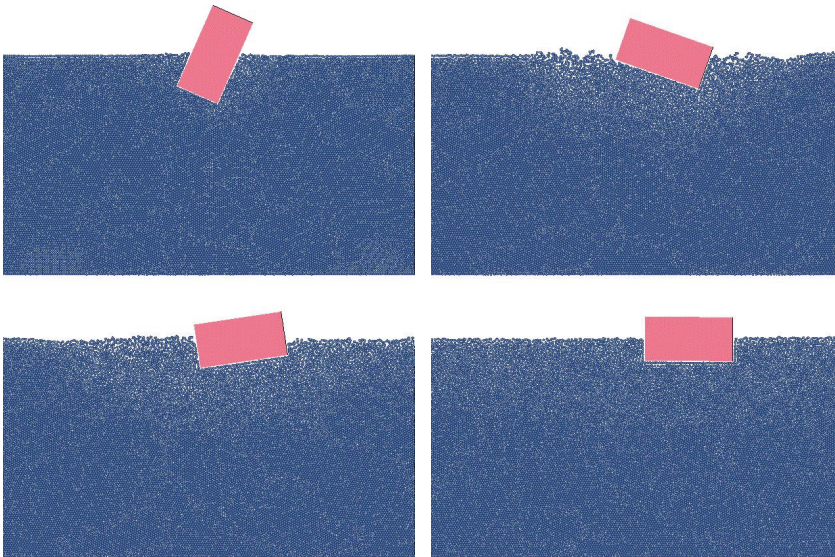


Figure 10: Four images showing rotation of the rectangular float during the simulation

The experiment was performed under the CAST (Crashworthiness of Helicopters on Water) EU Framework 5 project [Vigliotti (2003)]. The structure was manufactured from 2024 aluminum alloy and was characteristic of a typical metallic

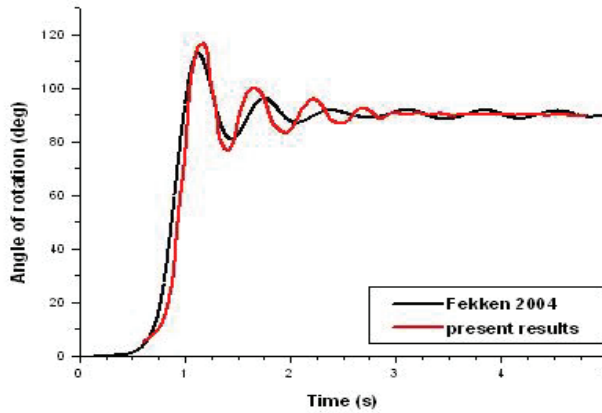


Figure 11: Time history for rotation angle of rectangular float

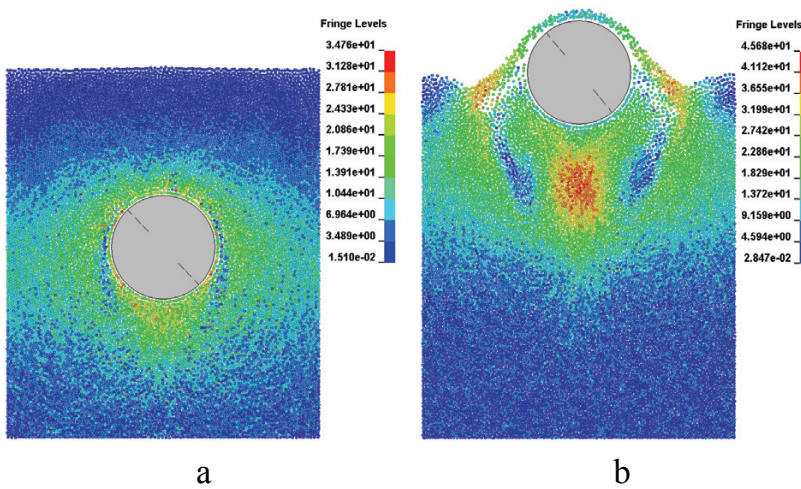


Figure 12: Rising cylinder simulation results at time 1.5 s (a) and time 3.0 s (b). The fluid particles show resultant velocity (m/s).

helicopter cabin sub-floor structure. In the experiment the structure was mounted on a trolley and dropped vertically onto water with an impact velocity of 7.95 m/s. The total mass on the structure and trolley was approximately 600 kg.

A finite element model of the sub-floor structure was constructed using shell elements. Material properties for the 2024 aluminum were taken from Johnson and Cook (1983). The trolley was represented as a rigid mass, and time history in-

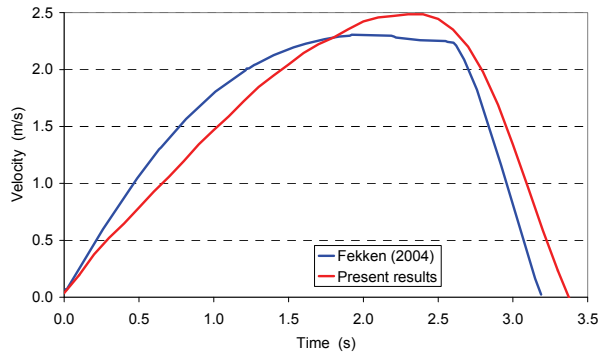


Figure 13: Vertical velocity of rising cylinder, compared with published results.

formation for the trolley acceleration was measured. The initial state of model is shown in figure 14 and consists of approximately 38000 shell elements and 61500 SPH particles. An element edge length of 1cm was used for the lower skin of the sub-floor. An initial inter-particle distance of 4cm was used for the SPH.

The overall deformation of the FE structure is consistent with the deformation observed in the experiment, figure 15. The test article shows a combination of plastic deformation, material failure and joint failure. The skin of the structure remains intact. No appropriate failure model was available to represent material failure in the FE model, so failure was ignored in the model. The locations of failure in the test are consistent with area of high plastic strain in the simulation results.

A comparison of the trolley acceleration results is shown in figure 15. A direct comparison of the results is difficult as the experimental results show that in the experiment the trolley and its supports were not fully rigid, unlike the representation of the trolley in the simulation. To correct this difference would require the addition of an FE model of the trolley which was not possible in this research. The peak acceleration levels are higher in the simulation but show a similar overall trend. The initial slope of the acceleration time curve from the simulation is higher than in the experiment as air is not included in the simulation. In the experiment there is an initial air cushion and a water-air mixture that can not be represented in the simulation. This difference is consistent with behavior observed in other water impact simulations [De Vuyst (2003)].

#### 4.4 Demonstration of wave response of a floating buoy.

The final simulation is a demonstration of the capability of the coupled approach to perform a 3D simulation of wave interaction with a floating body. The problem

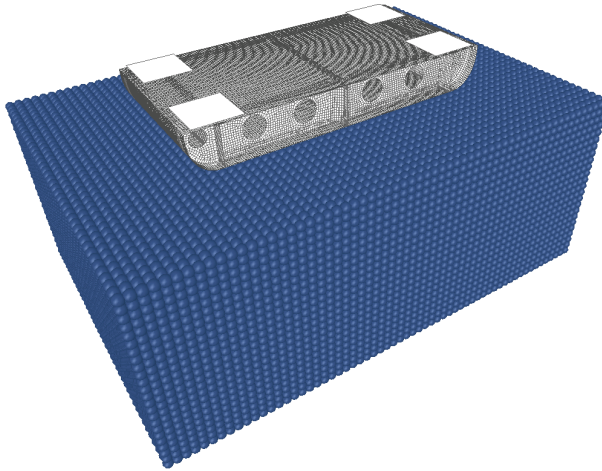


Figure 14: Initial model for helicopter sub-floor impact simulation.

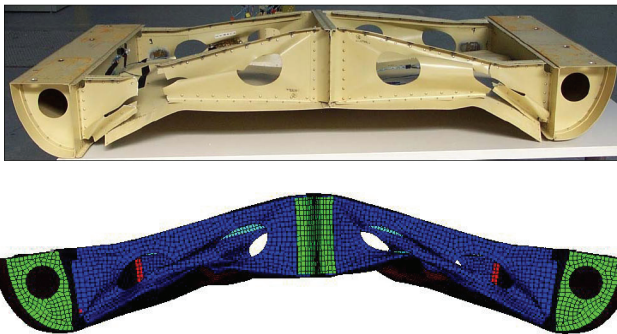


Figure 15: Comparison of deformed shape of test article and FE mesh.

consists of a free-floating cylindrical buoy of diameter 12 m and mass 400 tonnes. These dimensions are representative of an offshore mooring buoy. The buoy is modeled as a rigid material with appropriate inertial properties defined. The buoy geometry is represented by 504 shell elements with an average edge length of approximately 1m. The water volume is 111.75 m by 36 m by 28.5 m, modeled using 268,852 SPH particles. The initial inter-particle distance is 0.75m. The waves are generated using a wave maker, modeled as shell elements with a prescribed oscillating motion. Dynamic relaxation is used to determine the static solution to the initial pressure and contact equilibrium, figure 17.

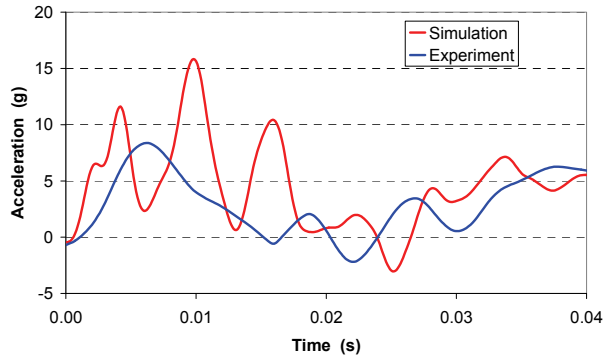


Figure 16: Comparison of trolley accelerometer data to simulation results.

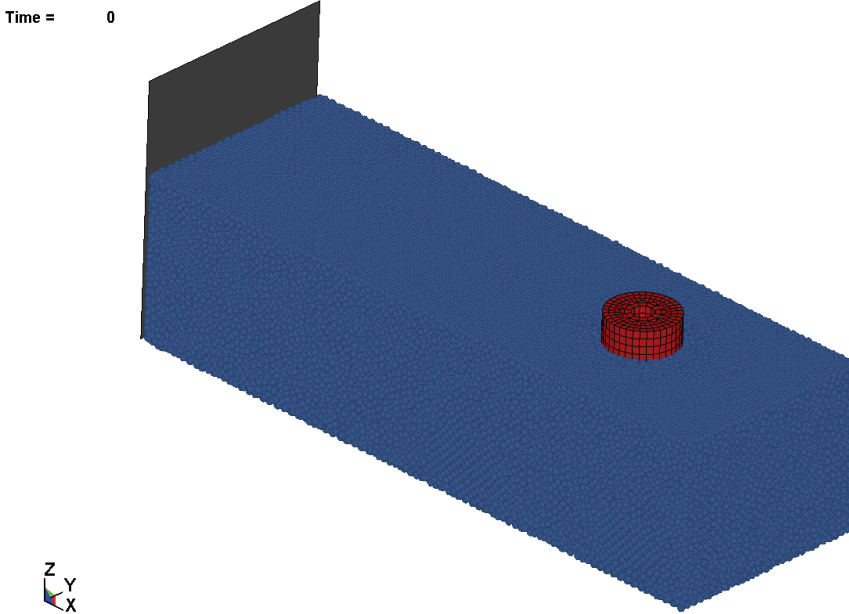


Figure 17: Initial state model for wave interaction with a floating buoy.

The simulation results show sensible behavior of the buoy as the waves pass, figure 18. As the buoy is free floating it is moved horizontally by the wave in the direction of the wave travel.

This simulation shows that the coupled FE-SPH approach can provide 3D predic-

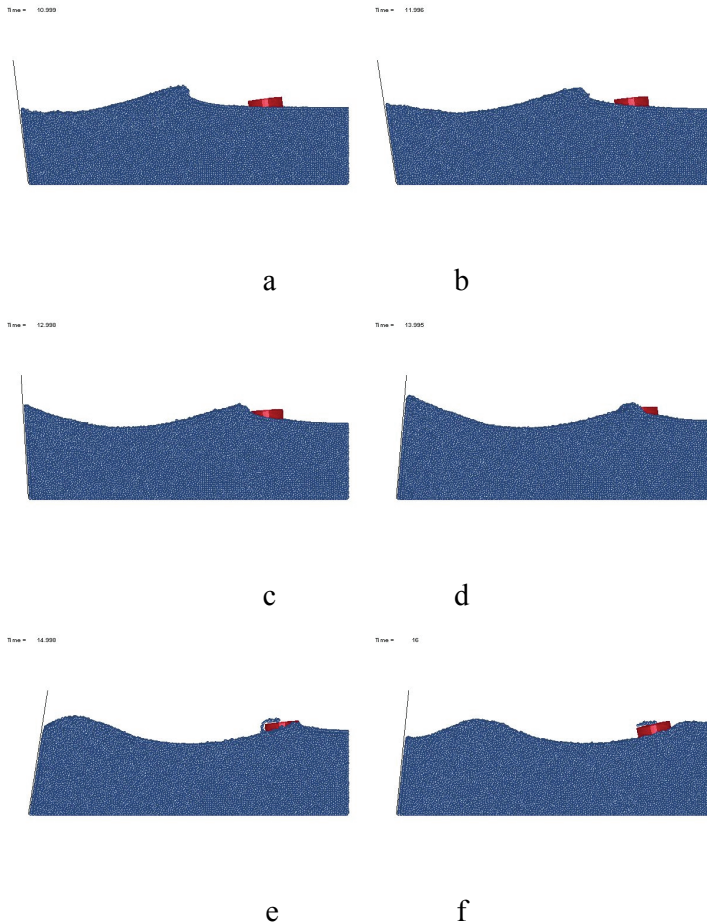


Figure 18: Sequence showing the interaction of the first large wave with the buoy. The wave amplitude is approximately 8 m. The images are 1 second apart.

tions for the behavior of a floating body. Further work is required to complete the validation of the capability and will consist of a model of a moored buoy under extreme wave loading, and comparison of the behavior with model test data. This will require a significantly larger water domain (in excess of 1 million SPH particles) to allow correct modeling of the waves, and the validation of an appropriate model of a catenary mooring line.

## 5 Conclusions

Extreme waves can cause significant damage to ships and offshore structures. Currently there is no reliable theoretical or numerical technique available to predict the relevant loads and structural response.

The coupled Finite Element – Smoothed Particle Hydrodynamics approach has been developed for treating fluid-structure interaction problems where the structural response is potentially highly non-linear. This paper demonstrates that the approach can be extended to the treatment of extreme wave loading of floating structures through the addition of appropriate initial and boundary conditions.

A set of simulation results are shown to demonstrate that the approach allows:

- the correct behavior of a floating body
- the prediction of structural collapse under water loading
- 3D simulation of wave interaction with a floating body

Further work is required to complete the demonstration and validation of this approach for this application.

**Acknowledgement:** The authors would like to acknowledge the support of the UK Engineering and Physical Sciences Research Council (EPSRC) under project GR/S95435/01.

## References

- Aliabadi, S.; Abedi, J.; Zellars, B.; Bota, K.; Johnson, A.** (2003) Simulation technique for wave generation. *Communications in Numerical Methods in Engineering*, vol. 19, pp. 349—359.
- Attaway, S.W.; Heinstein, M.W.; J.W. Swegle, J.W.** (1994) Coupling of smooth particle hydrodynamics with the finite element method. *Nuclear Engineering and Design*, vol. 150, pp. 199—205.
- Benz, W.** (1990) Smooth Particle Hydrodynamics: A review. In: J.R. Buchler, (ed), *The Numerical Modelling of Non-linear Stellar Pulsations*. Kluwer Academic Publishers, pp. 269-288.
- Buchner, B.; Bunnik, T.H.J.; Fekken, G.; Veldman, A.E.P.** (2001) A numerical study on wave run up on an FPSO bow. In: *Proceedings of OMAE2001: The 20th International conference on offshore mechanics and arctic engineering*. Rio de Janeiro, Brazil.

**Chikazawa, Y.; Koshizuka, S.; Oka, Y.** (2001) A particle method for elastic and visco-plastic structures and fluid structure interactions. *Computational Mechanics*, vol. 27, pp. 97—106.

**Crespo, A.J.C.; Gomez-Gesteira M.; Dalrymple R.A.** (2007) Boundary Conditions Generated by Dynamic Particles in SPH Methods. *Computers, Materials & Continua*, vol. 5, pp. 173-184.

**De Vuyst, T.** (2003) Hydrocode modeling of water impact. *PhD Thesis*, Cranfield University, UK.

**De Vuyst, T.; Vignjevic, R.; Campbell, J.C.** (2005) Coupling between meshless and finite element methods. *International Journal of Impact Engineering*, vol. 31, pp.1054-1064.

**Fekken, G.** (2004) Numerical simulation of free-surface flow with moving rigid bodies. *PhD Thesis*, Groningen University, Netherlands. Available online at: <http://irs.ub.rug.nl/ppn/260616745> (last accessed January 2009).

**Gingold, R.A.; Monaghan, J.** (1977) Smoothed particle hydrodynamics: Theory and application to non-spherical stars. *Monthly Notices of the Royal Astronomical Society*, vol. 181, pp. 375—389.

**Gómez-Gesteira, G.; Cerqueiro, D.; Crespo, C.; Dalrymple, R.A** (2005) Green water overtopping analyzed with a SPH model. *Ocean Engineering*, vol. 32, pp. 223-238.

**Hallquist, J.O.** (2006) LS-DYNA Theory Manual, Livermore Software Technology Corporation, USA.

**Johnson, G.R.; Cook, W.H.** (1983) A constitutive model and data for metals subjected to large strains, high strain rates and high temperatures. *Presented at: The Seventh International Symposium on Ballistics*. The Hague, Netherlands.

**Johnson, G.R.** (1994) Linking of Lagrangian particle methods to standard finite element methods for high velocity impact computations. *Nuclear Engineering and Design*, vol. 150, pp. 265—274.

**Kleefsman, K.M.T; Fekken, G.; Veldman, A.E.P.; Bunnik, T.H.J.; Buchner, B.; Iwanowski, B.** (2002) Prediction of green water and wave loading using a Navier-Stokes based simulation tool. In: *Proceedings of OMAE'02: 2002 ASME Offshore Mechanics and Arctic Engineering*, Oslo, Norway

**Koshizuka, S.; Nobe, A.; Oka, Y.** (1998) Numerical analysis of breaking waves using the moving particle semi-implicit method. *International Journal for Numerical Methods in Fluids*, vol. 26 pp. 751—769.

**Libersky, L.D.; Petschek, A.G.** (1990) Smooth Particle Hydrodynamics with strength of materials. In: H.E. Trease, M.J. Fritts, and W.P. Crowley (eds), *Advances in the*

*Free-Lagrange Method*. Springer-Verlag, pp. 248-257.

**Lin, J.I.** (1999) DYNA3D: A Nonlinear, Explicit, Three-Dimensional Finite Element Code for Solid and Structural Mechanics. User Manual. Lawrence Livermore National Laboratory, USA.

**Lo, E.Y.M.; Shao, S.** (2002) Simulation of near-shore solitary wave mechanics by an incompressible SPH method. *Applied Ocean Research*, vol. 24, pp. 275—286.

**Lucy, L.B.** (1977) A numerical approach to the testing of the fission hypothesis. *The Astronomical Journal*, vol. 82, pp. 1013—1024.

**Monaghan, J.** (1992) Smoothed Particle Hydrodynamics. *Annual Review of Astronomy and Astrophysics*, vol. 30, pp. 543—574.

**Monaghan, J.** (1994) Simulating free surface flows with SPH. *Journal of Computational Physics*, vol. 110, pp. 399—406.

**Moulinec, C.; Issa, R.; Marongiu, J.C.; Violeau, D.** (2008) Parallel 3-D SPH simulations. *CMES: Computer Modeling in Engineering and Sciences*, vol. 25, pp. 133-148.

**Shao, S.; Ji, C.; Graham, D.I.; Reeve, D.E.; James, P.W.; Chadwick, A.J.** (2006) Simulation of wave overtopping by an incompressible SPH model. *Coastal Engineering*, vol. 53, pp. 723-735.

**Tucker, M.J.; Pitt, E.G.** (2001). *Waves in Ocean Engineering*. Elsevier Science Ltd, Oxford, UK.

**Vigliotti, A.** (2003) Metallic specimen test report, D.6.5.1.2. CAST (Crashworthiness of helicopters on water: design of structures using advanced simulation tools). EU Framework V project, Contract G4RD-CT1999-01728, CIRA, Italy.

**Vignjevic, R.; De Vuyst, T.; Campbell, J.C.** (2006) A frictionless contact algorithm for meshless methods. *CMES: Computer Modeling in Engineering and Sciences*, vol. 13, pp. 35-47.

**Vignjevic, R.; Reveles, J.R.; Campbell, J.** (2006) SPH in a total Lagrangian formalism. *CMES: Computer Modeling in Engineering and Sciences*, vol. 14, pp. 181-198.

**Xie, H.; Koshizuka, S.; Oka, Y.** (2008) Modelling the wetting effects in droplet impingement using particle method. *CMES: Computer Modeling in Engineering and Sciences*, vol. 18, pp. 1-16.

